Temperature Dependence of the Photoisomerization of *cis*-1-(2-Anthryl)-2-phenylethene. Conformer-Specificity, Torsional Energetics and Mechanism

Jack Saltiel,* Yuxin Zhang, and Donald F. Sears, Jr.

Contribution from the Department of Chemistry, The Florida State University, Tallahassee, Florida 32306-3006

Received July 10, 1997[⊗]

Abstract: Emission from *cis*-1-(2-anthryl)-2-phenylethene, *c*-APE*, in toluene is resolved into ^1t-APE$_B$* and ^1c-APE* components at temperatures ranging between 4.3 and 59.3 °C. Decomposition of effective fluorescence quantum yields, $\bar{\phi}_{fc}$, into pure component fluorescence quantum yields, ϕ_{ft-B} and ϕ_{fc}, shows that ϕ_{ft-B} increases 24% with increasing temperature while ϕ_{fc} decreases more than 3-fold over this temperature range. On the basis of the fraction of molecules that escape the ^1c-APE* potential energy minimum, $1 - \phi_{fc}$, the efficiency of adiabatic formation of ^1t-APE$_B$* remains remarkably temperature independent at 50.5 ± 0.7%. These results, together with photoisomerization quantum yields as a function of [*c*-APE] in degassed and air-saturated toluene, reveal a detailed photoisomerization mechanism. At infinite dilution and in the absence of molecular oxygen, photoisomerization of *c*-APE occurs predominantly via the adiabatic, conformer-specific ^1c-APE$_B$* → ^1t-APE$_B$* pathway. This torsional motion experiences a $4.4_4 \pm 0.1_4$ kcal/mol barrier probably located at the perpendicular, ^{3}p*, geometry. Since 12% of ^1t-APE$_B$* intersystem cross to ^3t-APE$_B$*, the known triplet state quantum chain process enhances photoisomerization quantum yields at higher [*c*-APE]. Triplets formed directly from ^1c-APE* also contribute to this pathway. In air-saturated solutions, oxygen eliminates the quantum chain process by reducing the lifetime of ^3t-APE*. However, the quenching of ^1c-APE* by O_2 gives ^3c-APE*, thus enhancing photoisomerization quantum yields via rapid ^3c-APE* → ^3t-APE* adiabatic torsional displacement. No photoisomerization of ^1c-APE$_A$* need be postulated to account for our observations. The enthalpy difference between ground state conformers, ΔH_{AB}, favors *c*-APE$_B$ by 0.92 ± 0.02 kcal/mol.

Introduction

Olson proposed the first cis−trans photoisomerization mechanism of olefins in terms of potential energy curves.[1] He formulated the reaction as an adiabatic process in the excited state.[1a]

$$\text{molecule} + h\nu \rightarrow \text{molecule}' + h\nu' \qquad (1)$$

Mulliken's expansion[2] of Hückel's description of the double bond,[3] published nearly simultaneously with Olson's proposal, provided a quantum mechanical basis for the idea of barrierless rotation in the excited state. Lewis et al. reasoned that, if Olson's mechanism were correct, cis and trans olefins should exhibit identical fluorescence.[4] In a pioneering study of stilbene photoisomerization they searched in vain for *cis*-stilbene fluorescence. By establishing that the fluorescence intensity from *cis*-stilbene, if present, was less that 1% of the fluorescence of *trans*-stilbene, they showed that the contribution of an adiabatic pathway to stilbene photoisomerization is, at best, minor.[4]

Olson's mechanism lay dormant for over 40 years. It was resurrected in a series of papers starting in 1983 by Tokumaru and co-workers.[5] Adiabatic cis → trans photoisomerization in the lowest triplet state was shown to be the key step in the one-way photoisomerization of arylalkenes or of 1,2-diarylethylenes with a 2-anthryl substituent on the double bond, as in the title compound. The ^{3}c* → ^{3}t* process is followed by excitation transfer from ^{3}t* to a cis ground state molecule and a quantum chain process ensues.[5] This mechanism applies when the triplet energy of the aryl substituent of the arylalkene or of the diarylethylene is low relative to the energy of the corresponding perpendicular olefin triplet, ^{3}p*. Extensive localization of triplet excitation in the larger aryl substituent ensures that nearly planar transoid and cisoid olefin geometries correspond to energy minima in the triplet potential energy surface. The higher energy of ^{3}c*, due to steric hindrance, accounts for the ^{3}c* → ^{3}t* directionality of the process.

Adiabatic cis → trans photoisomerization in the lowest excited singlet state was reported four years later by Sandros and Becker for the 9-styrylanthracenes.[6] The emission of solutions of the cis isomer was shown to contain substantial contributions of fluorescence from the trans isomer. Other examples followed soon thereafter.[7−9] Our work has shown that, as the aryl substituent in *cis*-ArCH = CHPh derivatives is changed from

[⊗] Abstract published in *Advance ACS Abstracts,* November 1, 1997.

(1) (a) Olson, A. R. *Trans. Faraday Soc.* **1931**, *27*, 69−76. (b) Olson, A. R.; Hudson, F. L. *J. Am. Chem. Soc.* **1933**, *55*, 1410−1424. (c) Olson A. R.; Maroney, W. *J. Am. Chem. Soc.* **1934**, *56*, 1320−1322.

(2) Mulliken, R. S. *Phys. Rev.* **1932**, *41*, 751.

(3) Hückel, E. *Z. Phys.* **1930**, *60*, 423.

(4) Lewis, G. N.; Magel, T. T.; Lipkin, D. *J. Am. Chem. Soc.* **1940**, *62*, 2973−2980.

(5) (a) Arai, T.; Karatsu, T.; Sakuragi, H.; Tokumaru, K. *Tetrahedron Lett.* **1983**, *24*, 2873−2876. (b) Karatsu, T.; Arai, T.; Sakuragi, H.; Tokumaru, K. *Chem. Phys. Lett.* **1985**, *115*, 9−15. (c) Arai, T.; Karatsu, T.; Misawa, H.; Kuriyama, Y.; Okamoto, H.; Hiresaki, T.; Furuuchi, H.; Zeng, H.; Sakuragi, H.; Tokumaru, K. *Pure Appl. Chem.* **1988**, *60*, 989−998. (d) Tokumaru, K.; Arai, T. *J. Photochem. Photobiol. A* **1992**, *65*, 1−13. (e) Arai, T.; Tokumaru, K. *Chem. Rev.* **1993**, *93*, 23−39. (f) Tokumaru, K.; Arai, T. *Bull. Chem. Soc. Jpn.* **1995**, *68*, 1065−1087.

(6) (a) Sandros, K.; Becker, H.-D. *J. Photochem.* **1987**, 39, 301−315. (b) Görner, H. *J. Photochem. Photobiol. A* **1988**, *43*, 263−288. (c) Sandros, K.; Becker, H.-D. *J. Photochem. Photobiol. A* **1988**, *43*, 291−292.

(7) (a) Sandros, K.; Sundahl, M.; Wennerström, O.; Norinder, U. *J. Am. Chem. Soc.* **1990**, *112*, 3082−3086. (b) Sandros, K.; Sundahl, M.; Wennerström *J. Phys. Chem.* **1993**, *97*, 5291−5294. (c) Sandros, K.; Sundahl, M. *J. Phys. Chem.* **1994**, *98*, 5705−5708.

S0002-7863(97)02293-2 CCC: $14.00

Scheme 1

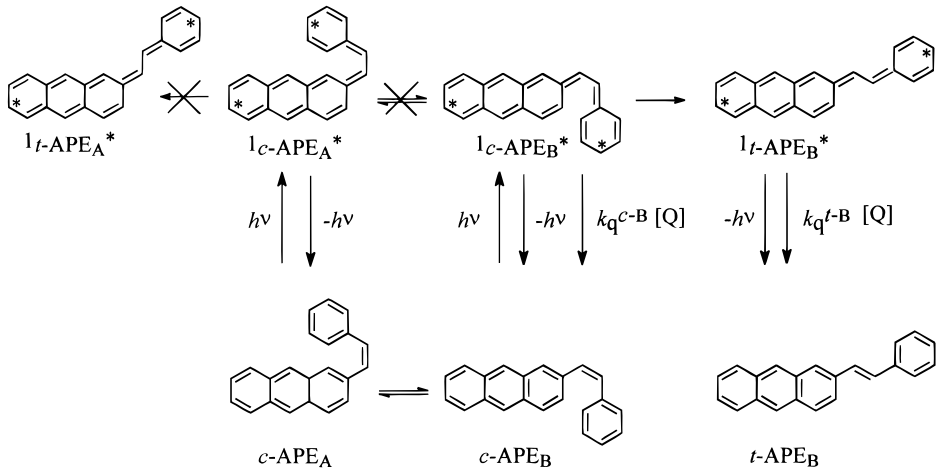

phenyl (Ph) to 2-naphthyl (2-Np) and then to 2-anthryl (2-An), the efficiency of the adiabatic $^1c^* \rightarrow {}^1t^*$ pathway increases from 0.2% to >2% and to >44%, respectively.[8] The greater localization of the electronic excitation in the largest aryl group is reflected in a 1000-fold increase in the fluorescence lifetime of *cis*-1-(2-anthryl)-2-phenylethene (*c*-APE) relative to *cis*-1-(2-naphthyl)-2-phenylethene (*c*-NPE).[8d,e] Moreover, the adiabatic photoisomerization pathway in these two molecules is highly conformer specific. As illustrated in Scheme 1 for *c*-APE, in each case, only the more extended conformers, *c*-NPE$_B$ and *c*-APE$_B$, exhibit the reaction.

In this paper we report the temperature dependence of the adiabatic ^1c-APE$_B^* \rightarrow {}^1t$-APE$_B^*$ process and the dependence of the photoisomerization quantum yield on [*c*-APE] under degassed and air-saturated conditions. These results provide insights concerning the energetics of $^1c^* \rightarrow {}^1t^*$ torsional motion in *c*-APE$_B$ and allow quantitative evaluation of the relative contributions of singlet and triplet excited states in cis−trans photoisomerization.

Experimental Section

Materials. Toluene, *c*-APE, and quinine sulfate were previously described.[8e] Fumaronitrile (Aldrich) was recrystallized from benzene prior to use. Fluorenone (Aldrich, 98%) was recrystallized from ethanol, chromatographed on alumina with benzene as eluent, and recrystallized twice from 95% ethanol (99.98% purity, GLC). *trans*-Stilbene (Aldrich, 96%) was recrystallized from ethanol, chromatographed on alumina with *n*-hexane as eluent, and sublimed under reduced pressure (99.99% purity, GLC). Benzene (Aldrich, Spectral grade) was passed through alumina prior to use.

Absorption Spectra. Absorption spectra were measured with a Perkin-Elmer Lambda-5 spectrophotometer interfaced with a 80486 DX (66 MHz) microcomputer.

Fluorescence Spectra. Fluorescence spectra were measured with an extensively modified Hitachi/Perkin-Elmer MPF-2A spectrophotometer as previously described.[10] All measurements were done under flow cell conditions with Ar-outgassed solutions.[8]

Photoisomerization Quantum Yields. A super-high-pressure mercury lamp (Bausch & Lomb SP-200) was used as the excitation source. The excitation wavelength, $\lambda_{exc} = 366$ nm, was selected with the use of a high-intensity grating mononochromator (Bausch & Lomb, 1200 grooves/mm). Incident light was beamed through an entrance slit into a dewar that contained a miniature aluminum merry-go-round apparatus in which five degassed Pyrex ampules (13 mm o.d.) containing different *c*-APE concentrations in toluene and a sixth ampule containing an actinometer solution were irradiated simultaneously. Samples were degassed by using 5 freeze−pump−thaw cycles to $\sim 3 \times 10^{-5}$ Torr and sealed at a constriction. Rotation of the merry-go-round was achieved by use of a GT21 motor (Gerald K. Heller Co.). The merry-go-round and samples were immersed in a water bath whose temperature was maintained at 19.3 ± 0.1 °C. Temperature was monitored by use of an Omega Engineering Model 199P2 RTD digital thermometer equipped with a HYP-4 RTD hypodermic probe. Irradiation periods were measured with a digital counter (Lab-CHRon). Different irradiation times were achieved by temporarily blocking the incident light beam.

Gas Chromatography. Actinometer solutions containing fluorenone and the stilbenes in benzene were analyzed by GLC (Varian 3300 gas chromatograph, equipped with a J&W Scientific DX-4 capillary column). The column temperature was programmed to increase from 160 to 180 °C at a rate of 1 °C/min. Injector and detector temperatures were maintained at 250 °C. The carrier gas (He) pressure was 12 psi. Integration of peak areas was achieved by use of a Varian 4290 integrator.

Data Analysis. Principal component analysis (PCA) calculations were performed on a Dell 80486/87 (25 MHz) microcomputer.

Results

Spectral Sets. Fluorescence spectra of *c*-APE in toluene were measured in a flow-cell system as a function of λ_{exc} and fumaronitrile, FN, concentration. Ar-saturated solutions were employed and measurements were recorded at 4.3, 39.3, and 59.3 °C. At each temperature toluene background spectra were recorded and then *c*-APE solution was added to a total volume of 200 mL. The concentration of FN was varied by successive additions of portions of a FN stock solution in toluene containing the identical *c*-APE concentration present in the circulating reservoir. Fresh solutions were employed for each temperature, and actual working concentrations of *c*-APE and FN were determined from UV absorption spectra by comparison with standard solutions.[11] Concentrations, corrected for solvent density variation with temperature, were as follows: at 4.3 °C, [*c*-APE] = 2.89×10^{-5} M, [FN] = 0.00, 1.43×10^{-3}, 3.84×10^{-3}, 7.91×10^{-3}, and 1.63×10^{-2} M; at 39.3 °C, [*c*-APE] =

(8) (a) Saltiel, J.; Waller, A.; Sun, Y.-P.; Sears, D. F., Jr. *J. Am. Chem. Soc.* **1990**, *112*, 4580−4581. (b) Saltiel, J.; Waller, A. S.; Sears, D. F., Jr. *J. Photochem. Photobiol. A* **1992**, *65*, 29−40. (c) Saltiel, J.; Waller, A. S.; Sears, D. F., Jr. *J. Am. Chem. Soc.* **1993**, *115*, 2453−2465. (d) Saltiel, J.; Tarkalanov, N.; Sears, D. F., Jr. *J. Am. Chem. Soc.* **1995**, *117*, 5586−5587. (e) Saltiel, J.; Zhang, Y.; Sears, D. F., Jr. *J. Am. Chem. Soc.* **1996**, *118*, 2811−2817.

(9) (a) Spalletti, A.; Bartocci, G.; Mazzucato, U.; Galiazzo, G. *Chem. Phys. Lett.* **1991**, *186*, 297−302. (b) Mazzucato, U.; Spalletti, A.; Bartocci, G. *Coord. Chem. Rev.* **1993**, *125*, 251−260. (c) Kikuchi, Y.; Okamoto, H.; Arai, T.; Tokumaru, K. *Chem. Phys. Lett.* **1994**, *229*, 564−570.

(10) Saltiel, J.; Sears, D. F., Jr.; Choi, J.-O.; Sun, Y.-P.; Eaker, D. W. *J. Phys. Chem.* **1994**, *98*, 35−46, 8260.

(11) Saltiel, J.; Zhang, Y.; Sears, D. F., Jr. *J. Phys. Chem.* **1997**, *101A*, 7053−7060.

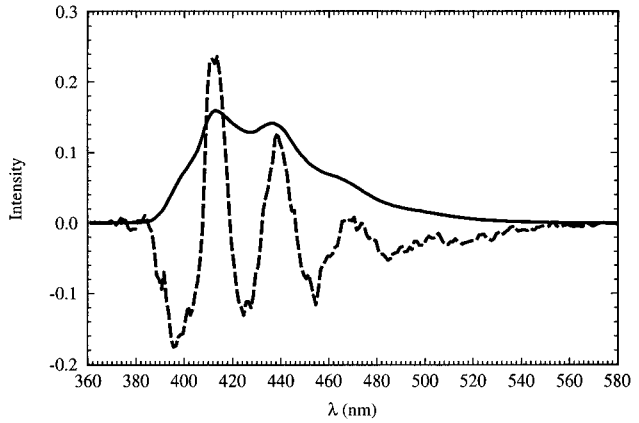

Figure 1. Eigenvectors of the *c*-APE/FN fluorescence matrix at 4.3 °C. The four largest eigenvalues are 0.137, 0.196 × 10^{-3}, 0.233 × 10^{-4}, and 0.912 × 10^{-5}.

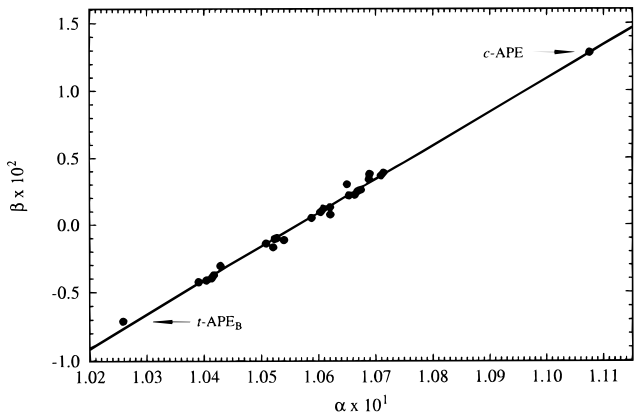

Figure 2. Normalization line based on the eigenvectors in Figure 1. The points are combination coefficients for experimental spectra and for pure component spectra (see arrows).

1.68 × 10^{-5} M, [FN] = 0.00, 1.93 × 10^{-3}, 4.04 × 10^{-3}, 5.90 × 10^{-3}, and 8.13 × 10^{-3} M; at 59.3 °C, [*c*-APE] = 2.92 × 10^{-5} M, [FN] = 0.00, 1.47 × 10^{-3}, 4.54 × 10^{-3}, 7.82 × 10^{-3}, and 1.08 × 10^{-2} M. Emission spectra were recorded in the 360−580-nm range in 0.5-nm increments with λ_{exc} = 350, 360, 380, 390, and 400 nm. A single spectrum was measured for each λ_{exc} and each [FN] yielding a (25 × 221) spectral matrix at each temperature. Comparison of absorption spectra before and after the fluorescence measurements showed no discernible changes in [*c*-APE].

Spectral Resolutions. Fluorescence spectra were corrected for background and self-absorption as previously described.[8e] PCA was applied separately to the 25 spectra at each temperature. Eigenvalues and eigenvectors from each matrix are consistent with two-component systems, as illustrated in Figure 1 for the 4.3 °C matrix. Spectral resolutions were achieved following the procedure described for O_2 quenching at 19.3 °C.[8e] The process relies on the previously determined *t*-APE_B spectra and Stern−Volmer (SV) constants for *t*-APE_B fluorescence by FN at each temperature.[11] The analysis at 4.3 °C is typical and is presented below in some detail. The combination coefficients of the known *t*-APE_B spectrum are defined by target analysis as dot products of this spectrum with the eigenvectors in Figure 1. They define a point that falls on the normalization line and corresponds to $K_{SV}^{c} = 62 \pm 2$ M^{-1} as the SV constant for FN quenching of *c*-APE fluorescence, Figure 2. On the basis of Scheme 1, the dependence of the fluorescence intensity of ^{1}*t*-APE_B* on [FN] should follow the quadratic relationship

$$\left(\frac{\phi_f^0}{\phi_f}\right)_{t-B} = (1 + K_{SV}^{c-B}[FN])(1 + K_{SV}^{t-B}[FN]) \quad (2)$$

where K_{SV}^{c-B} and K_{SV}^{t-B} are the SV constants for ^{1}*c*- and ^{1}*t*-APE_B*, respectively. Except for the substitution of quencher, eq 2 is identical with the equation employed for O_2 quenching.[8e] Proceeding as in the oxygen case, we assign the just determined $K_{SV}^{c} = 62$ M^{-1} value to ^{1}*c*-APE_B* and use the known value[11] of $K_{SV}^{t-B} = 266 \pm 6$ M^{-1} to define the expected FN quenching of ^{1}*t*-APE_B fluorescence based on eq 2. Location of the combination coefficients of *c*-APE on the normalization line is then based on reproducing the expected FN quenching curve, Figure 3. The resulting resolved *c*-APE fluorescence spectrum is shown in Figure 4 together with the spectra obtained at the other temperatures by following the same procedure. Stern−Volmer constants employed in the analyses and obtained for *c*-APE are shown in Table 1.

Fluorescence Quantum Yields. Fluorescence quantum yields for *c*-APE were determined under flow cell conditions with use of quinine bisulfate in 0.1 N H_2SO_4 as the fluorescence standard, $\phi_f = 0.546$.[12] Ar-saturated toluene solutions of *c*-APE, thermostated at the desired temperature, were employed and absorbances of standard and unknown were matched closely at λ_{exc}. All spectra were corrected for background and for nonlinearity in instrumental response. Fluorescence quantum yields, $\bar{\phi}_{fc}$, corrected for differences in index of refraction, are shown in Table 2. Bars over symbols indicate that measured quantities reflect composite behavior of a mixture of species. Estimated uncertainties in the quantum yields are ±3%.

Photoisomerization Quantum Yields. The fluorenone-sensitized photoisomerization of *trans*-stilbene in benzene was used for actinometry, $\phi_{tc} = 0.47$,[13,14] as previously described.[15] Conversions in actinometer solutions were corrected for back reaction.[16] Concentrations used for actinometry were [*t*-S] = 5.06 × 10^{-3} M and [Fl] = 2.87 × 10^{-2} M. Corrected actinometer conversions after 40.0 min of irradiation were 3.34 ± 0.03 and 3.65 ± 0.02% *cis*-stilbene for degassed and air-saturated *cis*-APE samples, respectively. Degassed and air-saturated *c*-APE solutions were irradiated for 2.0 and 8.0 min, respectively. Following irradiation, each *c*-APE solution was diluted and its UV absorption spectrum was recorded. Isomer compositions were determined on the basis of the entire spectrum by performing PCA on a matrix containing the absorption spectra of all irradiated solutions together with the spectra of pure *c*- and *t*-APE. Since the formation of *t*-APE is essentially irreversible, no back reaction correction is required. Observed conversions and corresponding photoisomerization quantum yields, $\bar{\phi}_{ct}$, are given in Table 3.

Discussion

PCA Resolution of *c*-APE Fluorescence. As described in the Results section, our resolution of *c*-APE fluorescence spectra into ^{1}*c*-APE* and ^{1}*t*-APE* components at different temperatures follows faithfully the procedure employed earlier for measurements at 19.3 °C.[8e] Substitution of FN for O_2 as the quencher avoids possible uncertainties in O_2 concentrations at different temperatures under our flow cell conditions. Earlier reports had shown that FN is a highly efficient quencher of the fluorescence

(12) Meech, S. R.; Phillips, D. *J. Photochem.* **1983**, *23*, 193−217.
(13) Caldwell, R. A.; Gajewski, R. P. *J. Am. Chem. Soc.* **1971**, *93*, 532.
(14) Valentine, D., Jr.; Hammond, G. S. *J. Am. Chem. Soc.* **1972**, *94*, 3449.
(15) Saltiel, F.; Dabestani, R.; Schanze, K. S.; Trojan, D.; Townsend, D. E.; Goedken, V. L. *J. Am. Chem. Soc.* **1986**, *108*, 2674−2687.
(16) Lamola, A. A.; Hammond, G. S. *J. Chem. Phys.* **1965**, *43*, 2129.

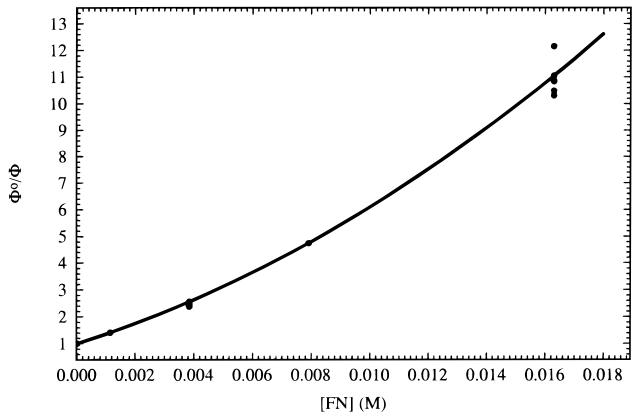

Figure 3. Global Stern−Volmer plot for FN quenching of *t*-APE$_B$ fluorescence at 4.3 °C. The curve is based on eq 2 with $K_{SVc-B} = 62$ M^{-1} and $K_{SVt-B} = 266$ M^{-1}.

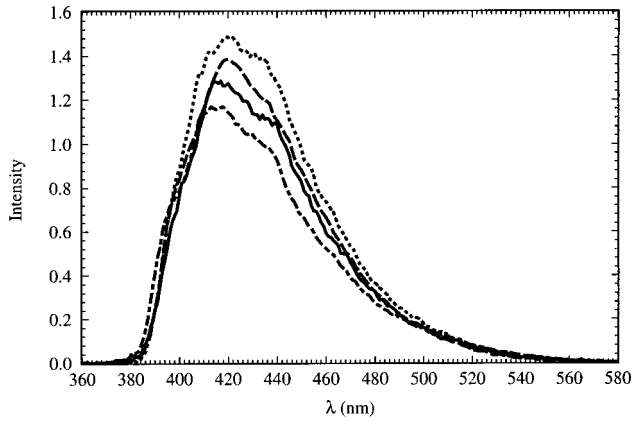

Figure 4. Arbitrarily scaled resolved *c*-APE fluorescence spectra obtained at 59.3, 39.3, 19.3, and 4.3 °C in the order of decreasing spectral area.

Table 1. Conformer-Specific SV Constants for FN Quenching of APE Fluorescence in Toluene[a]

	K_{SV}^{FN}, M^{-1}		
T, °C	*t*-APE$_A$[b]	*t*-APE$_B$[b]	*c*-APE$_B$
4.3	80.3(3.1)	265.9(5.5)	62(2)
19.3	116.0(6.0)	347.8(3.3)	57(4)[c]
39.3	155.2(5.7)	460.5(8.4)	50(3)
59.3	217.4(12.8)	547.5(21.5)	43(6)

[a] Values in parentheses are estimated uncertainties. [b] Reference 11. [c] Estimated, based on SV constants for FN and O_2 quenching of *t*-APE$_B$ and O_2 quenching of *c*-APE$_B$: $K_{SVc-B}^{FN} = K_{SVt-B}^{FN}(K_{SVc-B}^{OX}/K_{SVt-B}^{OX})$.

Table 2. The Temperature Dependence of Effective Fluorescence Quantum Yields from *c*-APE Solutions[a]

	$x_{t-B}(\lambda_{exc})$		$\bar{\phi}_{fc}(\lambda_{exc})$	
T, °C	350 nm	390 nm	350 nm	390 nm
4.3	0.585	0.580	0.56_9	0.48_8
19.3	0.718	0.723	0.53_1	0.45_6
39.3	0.805	0.808	0.50_5	0.42_3
59.3	0.853	0.833	0.48_4	0.39_7

[a] Toluene solvent; entries at 19.3 °C are from ref 8e.

of *trans*-stilbene[17] and of related 1,2-diarylethylenes,[18] and our work has established that FN and O_2 quench *t*-APE fluorescence at diffusion-controlled rates, showing no selectivity between *t*-APE$_A$ and *t*-APE$_B$.[11,19] Furthermore, the absence of fluorescence from potential *t*-APE/FN or *c*-APE/FN exciplexes renders the FN choice ideal for our resolutions as no additional fluorescent components are introduced.

Table 3. *c*-APE to *t*-APE Photoisomerization Quantum Yields[a] (Toluene, 19.3 °C)

degassed			air-saturated		
10^4[*c*-APE], M	x_t[b]	$\bar{\phi}_{ct}$	10^4[*c*-APE]	x_t[b]	$\bar{\phi}_{ct}$[c]
1.06	0.174	1.02(4)	1.05	0.341	0.55(2)
1.50	0.157	1.29(4)	1.45	0.282	0.62(2)
2.00	0.143	1.59(4)	1.99	0.200	0.57(2)
2.54	0.132	1.86(3)	2.25	0.182	0.58(2)
2.77	0.130	1.99(3)	2.67	0.151	0.56(2)

[a] Values in parentheses are estimated uncertainties in the last significant figure. They are based primarily on the uncertainty of the GLC analyses of actinometer solutions. [b] Observed fractional conversions to *t*-APE. [c] Photoisomerization quantum yields are corrected for light filtering by the product *t*-APE$_B$ by dividing effective quantum yields by $(1 - 0.5x_t)$, see text.

The resolved *c*-APE fluorescence spectra in Figure 4 are arbitrarily scaled to facilitate comparison. They are similar in shape, showing little, if any, vibronic structure. The blue shift, clearly evident at the onset of the 59.3 °C spectrum, may reflect the temperature-induced decrease in medium polarizability as discussed for the resolved conformer spectra of *t*-APE.[11] By analogy with *t*-APE,[19] we expect the *c*-APE$_A$ UV absorption spectrum to be somewhat red-shifted relative to the absorption spectrum of *c*-APE$_B$. This accounts for the sharp drop of $\bar{\phi}_{fc}$ when excitation is at the onset of the absorption spectrum of *c*-APE, from which an upper limit of $\phi_{fc-A} \leq 0.025$ at 19.3 °C was estimated.[8e] The effective fluorescence quantum yield of the *c*-APE component is larger by a factor of ≥5 than this upper limit in all spectra at 19.3 °C to which PCA was applied.[8e] Accordingly, the resolved *c*-APE fluorescence spectrum consists mainly of ^{1}*c*-APE$_B$* emission, at least for that temperature. The preponderance of ^{1}*c*-APE$_B$* fluorescence in the *c*-APE component at the other temperatures is indicated by the relative insensitivity to λ_{exc} of the location of the combination coefficients of the spectra on the normalization lines. The behavior at 4.3 °C, illustrated in Figure 2, where points for spectra for each [FN] appear as tight clusters on the normalization line, is typical.

SV Constants and the Lifetime of ^{1}*c*-APE$_B$*. Since the fluorescence of the *c*-APE component is associated mainly with the B conformer, the SV constants in Table 1 for *c*-APE likewise reflect mainly the quenching of ^{1}*c*-APE$_B$* and are so labeled. They decrease with increasing temperature, in sharp contrast with the SV constants of *t*-APE$_A$ and *t*-APE$_B$ that change strongly in the opposite direction. If FN quenching of *c*-APE fluorescence is diffusion controlled, as has been shown for the *t*-APE conformers,[11] then the difference between the temperature dependencies of the SV constants reveals the difference between the temperature dependencies of the fluorescence lifetimes of the *t*-APE conformers and of *c*-APE$_B$. The strong increases in the quenching rate constants k_{qt-A}^{FN}, k_{qt-B}^{FN}, and k_{qc-B}^{FN} with increasing *T* are evident in the K_{SV}^{FN} values of *t*-APE$_A$ and *t*-APE$_B$, whose fluorescence lifetimes are remarkably insensitive to temperature changes,[20] but are countered in K_{SVc-B}^{FN} by an

(17) (a) Green, B. S.; Rejtö, M.; Johnson, D. E.; Hoyle, C. E.; Simpson, J. T.; Correa, P. E.; Ho, T.-I.; McCoy, F.; Lewis, F. D. *J. Am. Chem. Soc.* **1979**, *101*, 3325−3331. (b) Lewis, F. D.; Simpson, J. T. *J. Phys. Chem.* **1979**, *83*, 2015−2019. (c) Hub, W.; Klüter, U.; Schneider, S.; Dörr, F.; Oxman, J. D.; Lewis, F. D. *J. Phys. Chem.* **1984**, *88*, 2308−2315.

(18) Aloisi, G. G.; Elisei, F.; Mazzucato, U.; Prats, M. *J. Photochem. Photobiol. A Chem.* **1991**, *62*, 217−228.

(19) Saltiel, J.; Zhang, Y.; Sears, D. F., Jr.; Choi, J.-O. *Res. Chem. Intermed.* **1995**, *21*, 899−921.

(20) (a) Bartocci, G.; Masetti, F.; Mazzucato, U.; Spalletti, A.; Orlandi, G.; Poggi, G. *J. Chem. Soc., Faraday Trans 2* **1988**, *84*, 385−399. (b) Bartocci, G.; Masetti, F.; Mazzucato, U.; Baraldi, I.; Fischer, E. *J. Mol. Struct.* **1989**, *193*, 173−183.

even stronger decrease in the lifetime of ^1c-APE$_B$*. Direct measurement of the fluorescence lifetime of *c*-APE in toluene at ambient temperature (~27 °C) has yielded $\tau_{fc} = 4.5 \pm 0.5$ ns,[8e] consistent with O_2 fluorescence quenching observations. Lifetimes at the temperatures employed in this work were estimated from the SV constants by assuming that k_{qc-B}^{FN} is roughly equal to the average of the known[11] k_{qt-A}^{FN} and k_{qt-B}^{FN} values

$$\tau_{fc-B} = \frac{2K_{SVc-B}^{FN}}{(k_{qt-A}^{FN} + k_{qt-B}^{FN})} \quad (3)$$

This approximation neglects differences in the small contributions of transient terms to the diffusion-controlled rate constants.[11,21] The resulting lifetimes are listed in Table 4. It is reassuring that the estimated value at 19.3 °C, $\tau_{fc-B} = 4.3$ ns, is well within experimental uncertainty of the measured value. If the FN quenching processes were all fully diffusion controlled, then these lifetimes would be slightly overestimated, as the transient term contribution to k_q is expected to be larger in shorter-lived species. The results show that τ_{fc-B} decreases by at least a factor of 3 as the temperature is increased from 4.3 to 59.3 °C.

Pure Component Fluorescence Quantum Yields and Rate Constants. Fractional contributions of *t*-APE$_B$ and *c*-APE fluorescence, $x_{t-B} + x_c = 1.00$, to the spectra on which the quantum yields in Table 2 are based were obtained by determining the location of (α,β) values for each spectrum on the normalization line for each temperature, e.g., Figure 2. Resulting fractional contributions, x_{t-B}, for 350- and 390-nm excitation are nearly identical, Table 2, at each temperature despite a 16−22% drop in $\bar{\phi}_{fc}$ at the longer wavelength. Since excitation at 390 nm is expected to increase the relative population of ^1c-APE$_A$*, this result is consistent with the conclusion that this conformer has a much smaller fluorescence quantum yield. On the basis of the fractional contributions, the effective fluorescence quantum yields are decomposed into pure component fluorescence quantum yields, Table 5. Neglecting incident light absorbed by *c*-APE$_A$ gives the minimum fractions of ^1c-APE$_B$* that reach ^1t-APE$_B$*, f_{ct^*},

$$f_{ct^*} = \frac{\phi_{ft-B}}{\phi_{ft-B}^0} \quad (4)$$

where $\phi_{ft-B}^0 = 0.88$ is the pure component fluorescence quantum yield of *t*-APE$_B$.[8e,11] Similarly, the minimum fractions of ^1c-APE$_B$* that escape radiationlessly the potential energy minimum at the cisoid geometry and adiabatically reach the potential energy minimum at ^1t-APE$_B$*, ϕ_{ct}^{esc}, are given by

$$f_{ct^*}^{esc} = \frac{\phi_{ft-B}}{\phi_{ft-B}^0(1 - \phi_{fc})} \quad (5)$$

In view of the temperature independence of τ_{ft-B}, Table 4,[20] ϕ_{ft-B}^0 is assumed to be similarly temperature independent. Equations 4 and 5 give minimum values for the desired quantities because the ϕ_{ft-B}'s are not corrected for incident light absorbed by *c*-APE$_A$. Fractions f_{ct^*} and $f_{ct^*}^{esc}$, based on the larger fluorescence quantum yields for $\lambda_{exc} = 350$ nm, are also listed in Table 5.

Table 5 reveals that ϕ_{fc} decreases sharply with increasing temperature (a factor of 3.3 in the 4.3 to 59.3 °C range for $\lambda_{exc} = 350$ nm), and that this decrease is concomitant with an increase in f_{ct^*}, the efficiency of the adiabatic ^1c-APE$_B$* → ^1t-APE$_B$* process. Furthermore, independent of temperature, fully 50.5 ± 0.5% of the initially excited *c*-APE molecules that do not decay radiatively reach ^1t-APE$_B$* on the excited state surface. It follows that radiative decay from ^1c-APE$_B$* competes with activated torsional motion to ^1t-APE$_B$*. We are left with the question of accounting for the remaining ~50% of excited *c*-APE molecules that decay radiationlessly but do not reach ^1t-APE$_B$*. Three possibilities are the following: (i) intersystem crossing to the triplet state from either ^1c-APE* conformer ($\phi_{isc} = 0.17$ has been reported[22]), (ii) competing excitation of relatively nonfluorescent *c*-APE$_A$, and (iii) diabatic photoisomerization from twisted ^1p_A* and ^1p_B* intermediates. Pathways i and iii can potentially contribute to the cis → trans photoisomerization process, and to the degree that this happens, observed quantum yields should exceed values predicted by the adiabatic ^1c-APE$_B$* → ^1t-APE$_B$* process. Pathway (i) should be reflected in [*c*-APE] dependent ϕ_{ct} values since APE triplets are known to photoisomerize via a quantum chain process in the $^3c^*$ → $^3t^*$ direction.[5] Such a concentration dependence was reported by Tokumaru and co-workers for the direct excitation photoisomerization of *c*-APE and was attributed entirely to path (i).[5c]

Photoisomerization Quantum Yields. Under degassed conditions, all $\bar{\phi}_{ct}$ values in Table 3 exceed unity. In addition, they are strongly [*c*-APE] dependent over the modest concentration range employed in our experiments. This behavior reflects the participation of triplets in the photoisomerization.[5] Neglecting, for the moment, the presence of two distinct conformers with conformer-specific rate constants, the simplest mechanism that accounts for the observations is given by the following sequence:

$$^1c\text{-APE} \xrightarrow{h\nu} {}^1c\text{-APE}^* \quad (6)$$

$$^1c\text{-APE}^* \xrightarrow{k_{fc}} {}^1c\text{-APE} + h\nu \quad (7)$$

$$^1c\text{-APE}^* \xrightarrow{k_{ct}^S} {}^1t\text{-APE}_B^* \quad (8)$$

$$^1c\text{-APE}^* \xrightarrow{k_{isc}} {}^3c\text{-APE}^* \quad (9)$$

$$^1t\text{-APE}^* \xrightarrow{k_{ft}} {}^1t\text{-APE} + h\nu \quad (10)$$

$$^1t\text{-APE}^* \xrightarrow{k_{ist}} {}^3t\text{-APE}^* \quad (11)$$

$$^3c\text{-APE}^* \xrightarrow{k_{ct}^T} {}^3t\text{-APE}^* \quad (12)$$

$$^3t\text{-APE}^* \xrightarrow{k_{dt}} {}^1t\text{-APE} \quad (13)$$

$$^3t\text{-APE}^* + c\text{-APE} \xrightarrow{k_{et}} {}^1t\text{-APE} + {}^3c\text{-APE}^* \quad (14)$$

Application of the steady state approximation on all excited species gives

$$\bar{\phi}_{ct} - f_{ct^*}\phi_{ft-B}^0 = (\bar{\phi}_{isc} + f_{ct^*}\phi_{ist-B}^0)(1 + k_{et}\tau_T[c\text{-APE}]) \quad (15)$$

where the subscripts *c* and *t* designate cis and trans isomers, respectively, and all other symbols have their usual meanings. The term $f_{ct^*}\phi_{ft-B}^0 = \phi_{ft-B}$ in eq 15 is the effective fluorescence quantum yield of *t*-APE$_B$ following 366-nm excitation of *c*-APE. Values of $\bar{\phi}_{fc}$ for $\lambda_{exc} = 340$, 350, 360, and 366 nm are in the narrow range of 0.49−0.53, and the fluorescence spectra for

(21) (a) Weller, A. *Z. Phys. Chem. NF* **1957**, *13*, 335−352. (b) Hui, M.-H.; Ware, W. R. *J. Am. Chem. Soc.* **1976**, *98*, 4718−4727.

Table 4. Fluorescence Lifetimes of *t*-APE and *c*-APE (Toluene)

	τ_f, ns		
T, °C	*t*-APE$_A$[a]	*t*-APE$_B$[a]	*c*-APE$_B$[b]
4.3	7.7	26.0	6.0
19.3	8.2	27.8	4.3
39.3	8.2	27.8	2.8
59.3	8.2	27.8	1.9

[a] By interpolation from ref 20. [b] Estimated by using eq 2.

Table 5. Species-Specific Quantum Yields

	$\phi_{ft-B}(\lambda_{exc})$		$\phi_{fc}(\lambda_{exc})$			
T, °C	350 nm	390 nm	350	390 nm	f_{ct*} (λ_{exc} = 350 nm)	f_{ct*}^{esc} (λ_{exc} = 350 nm)
4.3	0.33_3	0.28_3	0.23_6	0.20_5	0.37_8	0.49_5
19.3	0.38_1	0.33_0	0.15_0	0.12_6	0.43_3	0.50_9
39.3	0.40_5	0.34_2	0.09_8	0.08_1	0.46_1	0.51_1
59.3	0.41_3	0.33_1	0.07_1	0.06_6	0.46_9	0.50_5

these λ_{exc} are composed of essentially identical contributions of fluorescence from ^1c-APE* and ^1t-APE$_B$*.[8e] The average effective fluorescence quantum yield from adiabatically formed ^1t-APE$_B$* for these λ_{exc}'s, 0.383 ± 0.013,[8e] is in very good agreement with 0.381, the value found in this work for λ_{exc} = 350 nm at 19.3 °C, Table 5. This quantity represents the contribution of the singlet excited state adiabatic pathway to cis → trans photoisomerization that proceeds strictly according to Olson's eq 1. The right-hand side of eq 15 gives the total triplet contribution to the photoisomerization quantum yields. It consists of two terms since triplets form directly from ^1c-APE* and, following its adiabatic formation, from ^1t-APE$_B$*.

The derivation of eq 15 assumes that the $\bar{\phi}_{ct}$ values are based on negligibly small conversions to *t*-APE. Experimentally, the imposition of this condition would lead to highly inaccurate $\bar{\phi}_{ct}$ values. We have compromised by keeping conversions within the 13−17% range, Table 3. The *t*-APE product interferes in two ways. First, since 366 nm is very close to an isosbestic point of the APE isomers,[8e] *t*-APE acts as an internal filter and its presence leads to artificially low $\bar{\phi}_{ct}$ values. Second, this effect is alleviated somewhat because excitation of *t*-APE yields ^3t-APE*, albeit inefficiently, whose participation in eq 15 sensitizes the reaction. We can correct roughly for these effects by employing average concentrations: $[c\text{-APE}]_{avg} = (1 - 0.5x_t) \times [c\text{-APE}]_o$ and $[t\text{-APE}]_B = 0.5x_t[c\text{-APE}]_o$, where x_t is the observed fractional conversion to *t*-APE and the average fractional contributions of *c*- and *t*-APE are given by $x_{cavg} = (1 - 0.5x_t)$ and $x_{tavg} = 0.5x_t$. Equation 15 is modified to

$$(\bar{\phi}_{ct} - x_{cavg} f_{ct*}\phi^0_{ft-B}) = [x_{cavg}(\phi_{isc} + f_{ct*}\phi^0_{ist-B}) + x_{tavg}\bar{\phi}_{ist}] \times (1 + k_{et}\tau_T[c\text{-APE}]) \quad (16)$$

The plot of ($\bar{\phi}_{ct} - 0.38x_{cavg}$) vs the average concentration, $[c\text{-APE}]_{avg}$, is linear, Figure 5, $r = 0.9992$, and gives values of $0.11_8 \pm 0.02_6$ and (5.88 ± 0.13) × 10^3 M^{-1} for the intercept and slope, respectively. With the use of $\bar{\phi}_{ist} = 0.11$, measured by transient spectroscopy,[22] the intercept in Figure 5 gives ($\bar{\phi}_{ist} + f_{ct*}\phi^0_{ft-B}$) = 0.12 ± 0.03 as the overall triplet yield following excitation of *c*-APE. This value is probably well within experimental uncertainty of the reported value of 0.17 that was based on triplet−triplet absorption measurements in benzene.[22] The use of $\phi^0_{ist-B} = (1 - \phi^0_{ft-B}) = 0.12$ in eqs 15 and 16[8e,11] is justified because only ^1t-APE$_B$* is accessed adiabatically. Together with $f_{ct*} = 0.43$ from Table 5, it gives $\bar{\phi}_{isc} = 0.07 \pm 0.03$ as the effective intersystem crossing yield of *c*-APE at 19.3 °C. It follows that roughly 56% of the triplets of APE, formed following excitation of a *c*-APE solution, are populated from ^1c-APE*, a precursor with a ~4.4-ns lifetime, and the rest come from ^1t-APE$_B$*, a precursor with a 28-ns lifetime. The kinetics of the growth of triplet−triplet absorption starting from ^1c-APE* should reflect the decays of the two precursors, but have not been reported to date. It has been claimed, however, that the ^3c-APE* → ^3t-APE* process is too fast to be detected by transient triplet−triplet absorption measurements in the nanosecond time scale.[23] This conclusion is in good agreement with photoisomerization quantum yields in the presence of oxygen[5f,23] (see below).

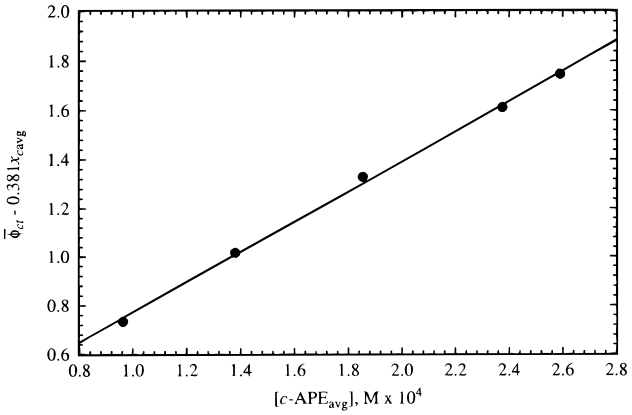

Figure 5. The dependence of $\bar{\phi}_{ct}$ on $[c\text{-APE}]_{avg}$ at 19.3 °C in toluene (see eq 16).

The slope to intercept ratio of the plot in Figure 5 gives $k_{et}\tau_T$ = (5.0 ± 1.3) × 10^4 M^{-1}, for toluene at 19.3 °C. This is considerably larger than the value of ~1 × 10^4 M^{-1} estimated on the basis of the dependence of $\bar{\phi}_{ct}$ on [*c*-APE] in benzene under direct and biacetyl-sensitized excitation conditions.[23] Some of the discrepancy is deceiving as it reflects primarily the fact that the adiabatic photoisomerization pathway in S_1 was not taken into account in the earlier treatment of the direct excitation results. In particular, our results are in reasonable agreement with those obtained for the direct excitation of *c*-APE in benzene by Arai et al.[5e,f] Their plot of $\bar{\phi}_{ct}$ vs [*c*-APE] gave $i = 0.43$ and $s = 4.2 \times 10^3$ M^{-1}.[23] Our data plotted in the same way give $i = 0.43_7 \pm 0.02_6$ and $s = (5.6 \pm 0.1) \times 10^3$ M^{-1}. The difference in slope could reflect interference by residual O_2 in the Ar-outgassed solutions employed in the earlier work. The effect of residual O_2 should be negligible on the adiabatic singlet photoisomerization pathway and should not influence the intercept of the plot as is observed. Identical triplet transient absorption spectra, assigned to ^3t-APE*, have been reported 20 and 90 μs following the excitation pulse starting from either *c*-APE or *t*-APE.[5b] Under degassed conditions in benzene, the triplet lifetime is $\tau_T = 190$ μs.[5b] On the basis of this lifetime, our results give $k_{et} = 2.6 \times 10^8$ M^{-1} s^{-1} for the propagation step of the quantum chain process. We note that, under Ar-outgassed conditions, incomplete O_2 removal can lead to significantly smaller triplet lifetimes. The longest reported lifetime obtained for ^3t-APE* in benzene with Ar outgassing is 117 μs,[24] and Tokumaru and co-workers have used both 190 μs[5c] and 30 μs[23] for τ_T in alternative interpretations of their data.

Participation of ^3t-APE as the chain carrier for photoisomerization via the quantum chain process is eliminated in air-saturated benzene or toluene solutions because O_2 quenching

(22) Arai, T.; Karatsu, T.; Tsuchiya, M.; Sakuragi, H.; Tokumaru, K. *Chem Phys. Lett.* **1988**, *149*, 161−166.

(23) Karatsu, T.; Tsuchiya, M.; Arai, T.; Sakuragi, H.; Tokumaru, K. *Bull. Chem. Soc. Jpn.* **1994**, *67*, 3030−3039.

diminishes τ_T by about 1000-fold.[5b,24] This accounts for the sharp decrease in $\bar{\phi}_{ct}$ of *c*-APE that was observed at very low $[O_2]$ in benzene.[5b] Starting from $\bar{\phi}_{ct} = 2.1$ under O_2-free conditions, the quantum yield drops to ~0.59 at $[O_2] \simeq 4 \times 10^{-4}$ M and appears to roughly plateau there at higher $[O_2]$.[5b] The fact that $\bar{\phi}_{ct}$ remains as high as 0.50 at $[O_2] = 7.7 \times 10^{-3}$ M, the highest $[O_2]$ employed, was a puzzle to Tokumaru and Arai[5b] because they were unaware of the singlet excited state photoisomerization pathway. On the basis of our mechanism, O_2 may interfere with cis → trans photoisomerization only by quenching *c*-APE excited states

$$^1c\text{-APE}^* + {}^3O_2 \xrightarrow{k_{qox}^T} {}^3c\text{-APE}^* + {}^1O_2^* \text{ or } {}^3O_2 \qquad (17)$$

$$^3c\text{-APE}^* + {}^3O_2 \xrightarrow{k_{qox}^S} {}^1c\text{-APE}^* + {}^1O_2^* \text{ or } {}^3O_2 \qquad (18)$$

Since O_2 eliminates the quantum chain process, quenching of ^1t-APE_B* or ^3t-APE_B* has no effect on $\bar{\phi}_{ct}$, except that it eliminates sensitization of the reaction by the product, *t*-APE.

Quenching of ^1c-APE* in toluene at 19.3 °C occurs with $K_{SVc}^{OX} = 160 \pm 15$ M^{-1}.[8e] Transient spectroscopic measurements, using nanosecond time resolution, indicate that ^3c-APE* → ^3t-APE* occurs too rapidly to be quenched by O_2 in air-saturated solutions.[5f] For this limiting case, O_2 interferes with unimolecular *c*-APE photoisomerization only by quenching ^1c-APE* and the quantum yield is given by

$$\bar{\phi}_{ct} = \frac{f_{ct^*} + \phi_{isc} + K_{SVc}[O_2]}{1 + K_{SVc}[O_2]} \qquad (19)$$

At the other extreme is the case for which O_2 quenches all ^3c-APE*, effectively shutting down its adiabatic photoisomerization by eq 14. For this case, the photoisomerization quantum yield is given by

$$\bar{\phi}_{ct} = \frac{f_{ct^*}}{1 + K_{SVc}[O_2]} \qquad (20)$$

Both eqs 19 and 20 are consistent with our observation that $\bar{\phi}_{ct}$ is independent of [*c*-APE] in air-saturated toluene, Table 3. Since all parameters in these equations are known, we can readily calculate $\bar{\phi}_{ct} = 0.61$ and 0.34 for none of ^3c-APE* quenched (eq 19) and for all of ^3c-APE* quenched (eq 20), respectively. The average experimental value for air-saturated toluene solutions, $\bar{\phi}_{ct} = 0.58 \pm 0.03$, is in excellent agreement with the value predicted for negligible ^3c-APE* quenching by O_2, eq 19, confirming the conclusion of Tokumaru and co-workers that the ^3c-APE* → ^3t-APE* process is nearly barrierless in fluid solutions.[5f] Our photoisomerization quantum yield in the presence of air in toluene is also in excellent agreement with Tokumaru's observations in benzene.[5f]

We stress that the photoisomerization quantum yields in Table 3 are accounted for, nearly quantitatively, without the necessity of postulating additional photoisomerization pathways involving twisted singlet excited state intermediates from either conformer, ^1p_A* or ^1p_B*. *All photoisomerization in c-APE singlet excited states proceeds via the conformer-specific adiabatic pathway shown in eq 5.* All other photoisomerization events involve triplet states that are formed inefficiently by intersystem crossing from ^1c-APE* and ^1t-APE_B*, $\phi_{isc} = 0.07$ and $\phi_{ist-B} = 0.12$. Thus following *c*-APE excitation at 366 nm in toluene at 19.3 °C fully 43% of ^1c-APE* isomerize via the ^1c-APE_B* → ^1t-APE_B* pathway, 15% fluoresce, and ~7% undergo intersystem crossing. The radiationless decay pathways that account for the remaining one-third of excited *c*-APE molecules do not contribute to cis → trans photoisomerization and may involve cyclization to dihydrophenanthrenes, particularly from ^1c-APE_A*.[25]

Table 6. The Temperature Dependencies of Limiting Rate Constants for Radiative and Radiationless Decay of ^1c-APE* [a]

T, °C	$10^{-8}k_{ct+}^s$, s^{-1}	$10^{-8}k_{ct-}^s$, s^{-1}	$10^{-7}k_{fc-}$, s^{-1}
4.3	1.27	0.63	3.9
19.3	1.99	1.01	3.5
39.3	3.20	1.64	3.5
59.3	4.99	2.52	3.8

[a] Quantum yields for $\lambda_{exc} = 350$ nm were employed.

The Energy Barrier for Torsional Motion in ^1c-APE_B*. Semiempirical quantum mechanical calculations predict that the perpendicular geometry, ^1p_A*, of the singlet excited state of APE_A is a transition state along the ^1c-APE_A* → ^1t-APE_A* reaction coordinate 16 kcal/mol above the energy of ^1c-APE_A*.[20a] This prediction is consistent with the absence of photoisomerization via this reaction coordinate, including the inaccessibility of ^1p_A* as a potential intermediate. No such calculations have been reported for APE_B. However, on the basis of the rate constant for radiationless decay of ^1c-APE_B* in toluene in 19.3 °C, the activation energy barrier along the ^1c-APE_B* → ^1t-APE_B* reaction coordinate was estimated as ≤7 kcal/mol.[8e] Quantitative evaluation of this barrier can now be based on the temperature dependencies of the fluorescence lifetime of *c*-APE, Table 4, and of the resolved fluorescence quantum yields, Table 5. Sums of all nonradiative decay rate constants, k_{nrc}, of *c*-APE are given by $(1 - \bar{\phi}_{fc})/\tau_{fc}$. In addition to k_{ct}^s, k_{nrc} includes radiationless decay via intersystem crossing as well as all other radiationless decay pathways of both conformers. The k_{nrc} values set a maximum limit on k_{ct}^s and are listed in the k_{ct+}^s column in Table 6. Since the fraction of incident light absorbed by *c*-APE_A is unknown, minimum values of k_{ct}^s can be estimated from f_{ct^*}/τ_{fc}. These values are listed in the k_{ct-}^s column in Table 6. Also listed in Table 6 are minimum values of k_{fc} based on $\bar{\phi}_{fc}/\tau_{fc}$. It is gratifying that k_{fc} is temperature independent, within experimental uncertainty, whereas k_{ct+}^s and k_{ct-}^s both decrease by a factor of 4 upon decreasing the temperature from 59.3 °C to 4.3 °C. The k_{ct+}^s/k_{ct-}^s ratio is 2.0, independent of temperature. Both sets of k_{ct}^s values in Table 6 adhere nicely to Eyring's transition state equation

$$\ln(k_{ct}^s/T) = \ln\left(\frac{\kappa k}{h}\right) + \frac{\Delta S_{ct}^{\ddagger}}{R} - \frac{\Delta H_{ct}^{\ddagger}}{R} \qquad (21)$$

where $\Delta H_{ct}^{\ddagger}$ is the enthalpy of activation, $\Delta S_{ct}^{\ddagger}$ is the entropy of activation, and κ is a transmission factor. Plots of k_{ct+}^s and k_{ct-}^s vs *T* based on eq 21 are shown in Figure 6. The two lines are astonishingly parallel, giving $\Delta H_{ct-}^{\ddagger} = 3.99 \pm 0.12$ and $\Delta H_{ct+}^{\ddagger} = 3.93 \pm 0.007$ kcal/mol from k_{ct-}^s and the k_{ct+}^s plots, respectively. Since k_{ct+}^s includes substantial contributions from all the other radiationless decay processes, including those of ^1c-APE_A*, two possible explanations for this slope coincidence are (i) all other radiationless decay pathways, coincidentally, have the same activation energies as does k_{ct}^s and (ii) f_{ct^*} and ϕ_{fc} account for all ^1c-APE_B* decay.

(24) Wismontski-Knittel, T.; Das, P. K. *J. Phys. Chem.* **1984**, *88*, 1168−1173.

(25) Laarhoven, W. H.; Cuppen, Th. J. H. M.; Nivard, R. J. F. *Tetrahedron* **1970**, 4865−4881.

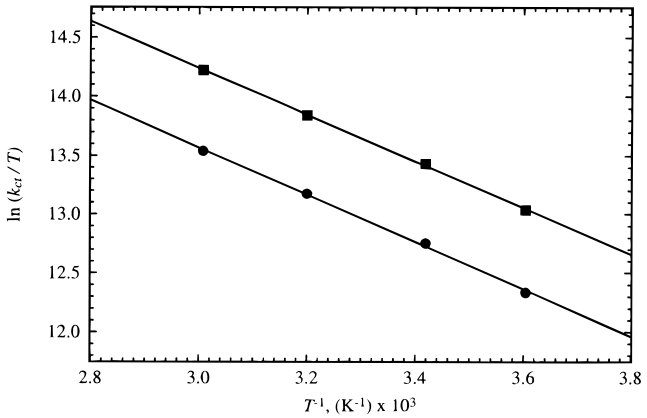

Figure 6. Transition state plots for k^s_{ct+} (■) and k^s_{ct-} (●).

Table 7. The Temperature Dependencies of Quantum Yields and Rate Constants for ^1c-APE_B* [a]

	$\phi_{ct-B^*}(\lambda_{exc})$			
T, °C	350 nm	390 nm	$10^{-8}k^s_{ct}$, s^{-1}	$10^{-7}k_{fc-B}$, s^{-1}
4.3	0.61_6	0.61_1	1.03	6.4
19.3	0.74_3	0.74_8	1.74	6.0
39.3	0.82_5	0.82_8	2.93	6.2
59.3	0.87_7	0.85_1	4.72	6.6

[a] See text for assumptions; rate constants are based on $\lambda_{exc} = 350$ nm data.

The second explanation appears more attractive. Normalized f_{ct^*} and ϕ_{fc} values were obtained by dividing each by the corresponding ($f_{ct^*} + \phi_{fc}$) sum. This procedure neglects small contributions of ^1c-APE_A* to ϕ_{fc}. The validity of the assumption that fluorescence from ^1c-APE_A* contributes negligibly to ϕ_{fc} for $\lambda_{exc} \leq 390$ nm is confirmed by the fact that the two sets of normalized f_{ct^*} values, derived independently from the $\lambda_{exc} =$ 350 and 390 nm data, are nearly identical, Table 7 (normalized f_{ct^*} values are labeled ϕ_{ct-B^*} in Table 7). The resulting conformer specific rate constants are also shown in Table 7. The transition state plot for k_{ct^*}, Figure 7, gives $\Delta H_{ct}^{\ddagger} = 4.44 \pm 0.14$ kcal/mol and, with $\kappa = 1$, $\Delta S_{ct}^{\ddagger} = -5.7 \pm 0.5$ eu. The calculated k_{fc-B} value, $(6.3 \pm 0.3) \times 10^7$ s^{-1}, is temperature independent as expected.[26] However, because the overall intersystem crossing yield of *c*-APE is low, the other extreme model for which only ^1c-APE_B* gives triplets also leads to a reasonable fit of the data.[26]

Ground State Conformer Equilibration in *c*-APE. The difference in slopes between the plots in Figures 6 and 7 is significant. Temperature changes affect both k^s_{ct} and the equilibrium fraction of *c*-APE_B in the conformer mixture. The raw quantum yields employed to generate $k^s_{ct\pm}$ and the plots in Figure 6 reflect both of these changes. Since we have shown that *c*-APE_A fluorescence is negligible for $\lambda_{exc} \leq 390$ nm, all fluorescence arises from the fraction of excited *c*-APE_B molecules, f_{c-B},

$$f_{c-B} = \frac{\epsilon_{c-B}[c\text{-APE}_B]}{\epsilon_{c-A}[c\text{-APE}_A] + \epsilon_{c-B}[c\text{-APE}_B]} \qquad (22)$$

where ϵ_{c-A} and ϵ_{c-B} are the molar absorptivities of *c*-APE_A and *c*-APE_B at a specified λ_{exc}, respectively. The relationship between the f_{ct}* values in Table 5 and the ϕ_{ct-B} values in Table 7 is given exactly by

$$f_{ct}^* = f_{c-B}\phi_{ct-B} \qquad (23)$$

Substitution of eq 22 into eq 23 and rearrangement gives

$$\ln\left(\frac{\phi_{ct-B}}{f_{ct}^*} - 1\right) = \ln\frac{\epsilon_{c-A}}{\epsilon_{c-B}} + \ln K_{AB} = \ln\frac{\epsilon_{c-A}}{\epsilon_{c-B}} + \frac{\Delta S_{AB}}{R} - \frac{\Delta H_{AB}}{RT} \qquad (24)$$

where K_{AB} is the equilibrium constant for *c*-$APE_B \rightleftharpoons$ *c*-APE_A conformer interconversion and ΔS_{AB} and ΔH_{AB} are the ground state entropy and enthalpy differences between *c*-APE_A and *c*-APE_B. Plots for the $\lambda_{exc} = 350$ and 390 nm data, based on eq 24, Figure 8, are parallel and linear ($|r| = 0.9953$ and 0.9997, respectively), and their slopes give $\Delta H_{AB} = 0.91 \pm 0.06$ and 0.93 ± 0.02 kcal/mol, respectively. It follows that *c*-APE_B is 0.92 ± 0.04 kcal/mol more stable than *c*-APE_A, consistent with the conclusion that the more extended B conformer is similarly more stable in *t*-APE.[19,20,27] Neglecting entropy differences, this energy difference predicts a small variation in the percent [*c*-APE_B] in the temperature range employed (from 84.0% to 80.0% as the temperature is increased from 4.3 to 59.3 °C).

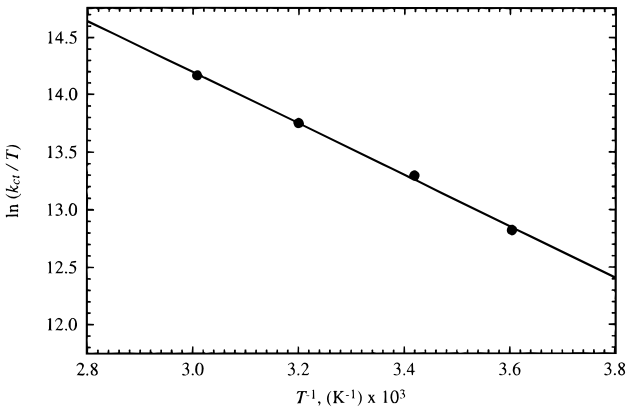

Figure 7. Transition state plot for k^s_{ct}.

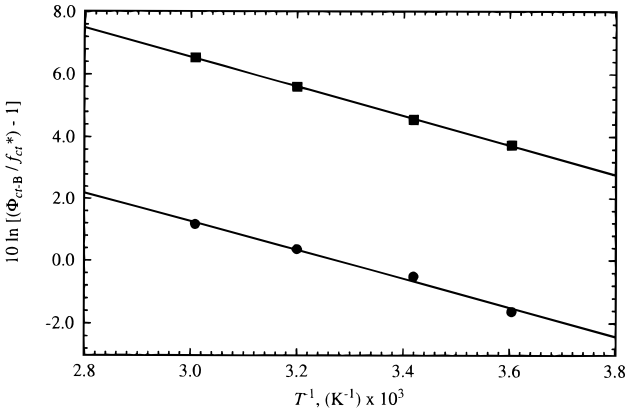

Figure 8. The temperature dependence of K_{AB}, the *c*-$APE_B \rightleftharpoons$ *c*-APE_A equilibrium constant based on $\lambda_{exc} = 350$ (●) and 390 nm (■).

Potential Energy Surface. A self-consistent interpretation of the data has emerged based on the assumption that essentially all ^1c-APE_B* molecules that do not fluoresce undergo adiabatic photoisomerization to ^1t-APE_B* over a 4.4 kcal/mol torsional

(26) At the other extreme is the model that assigns all intersystem crossing to ^1c-APE_B* and leads to $k_{isc-B} = 2.3_8 \times 10^7$ s^{-1} at 19.3 °C. With the further assumption that k_{isc-B} is temperature independent, the 350-nm data give $\Delta H_{ct}^{\ddagger} = 4.73 \pm 0.16$ kcal/mol and, with $\kappa = 1$, $\Delta S_{ct}^{\ddagger} = -5.0 \pm 0.5$ eu. However, k_{fc-B} is now predicted to increase systematically from 5.5×10^7 to 6.8×10^7 s^{-1} as the temperature is raised from 4.3 to 59. 3 °C.

(27) (a) Bartocci, G.; Mazzucato, U.; Spalletti, A.; Elisei, F. *Spectrochim. Acta, A* **1990**, *46*, 413−418. (b) Spalletti, A.; Bartocci, G.; Masetti, F.; Mazzucato, U.; Cruciani, G. *Chem. Phys.* **1992**, *160*, 131−144.

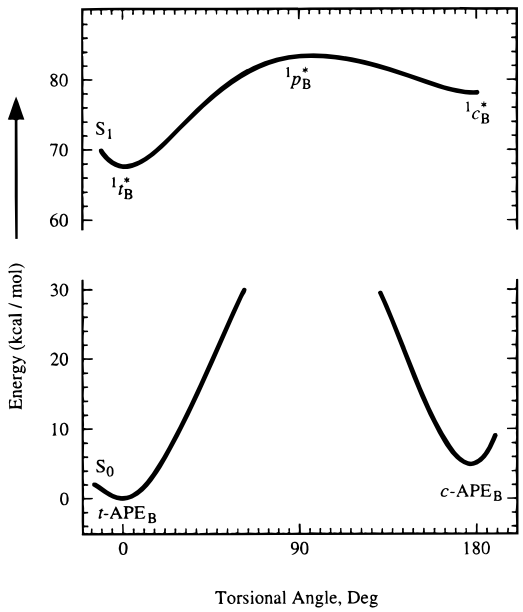

Figure 9. Proposed potential energy curve for the ^1c-APE$_B$* → ^1t-APE$_B$* reaction.

barrier. The energy difference between the ground states of *t*-APE$_B$ and *c*-APE$_B$ has been attributed to the steric interaction of the ortho hydrogens in the cis isomer and is roughly assigned[5] the value of 5 kcal/mol as in stilbene.[28] The origins of *t*-APE and *c*-APE $S_1 \leftarrow S_0$ transitions had been assigned values of 70.2 and 71.3 kcal/mol, respectively, on the basis of unresolved spectra.[5f] We assign values of 67.6 and 73.3 kcal/mol for *t*-APE$_B$ and *c*-APE$_B$, respectively, on the basis of our resolved fluorescence and absorption spectra.[8e,11,19] The resulting potential energy curve for the ^1c-APE$_B$* → ^1t-APE$_B$* torsional coordinate is shown in Figure 9. It accounts nicely for the absence of trans → cis photoisomerization in S_1 of APE$_B$ as this process faces an insurmountable 15 kcal/mol activation barrier. In principle, a shallow minimum cannot be ruled out at ^{1}p$_B$*. However, the data require that any residence time at that geometry be insufficient to allow radiationless decay from there to contribute to cis → trans photoisomerization.

The radiative lifetime of S_1 of *t*-APE$_B$ is at least 32 ns, as the usual τ_f/ϕ_f calculation neglects contributions to these quantities by the more allowed $S_2 \rightarrow S_0$ emission.[11,20b,27] On the basis of our estimated k_{fc-B}, Table 7, the radiative lifetime of ^1c-APE$_B$* is smaller by at least a factor of 2. Thus, the cis → trans process in S_1 appears to involve passing from a more allowed cis electronic state to a more forbidden trans electronic state. This difference in the nature of the electronic states of the two isomers may render $\kappa < 1$ in eq 21 and may account for the negative activation entropy that results when $\kappa = 1$ is assumed.

Concluding Remarks. In the lowest excited singlet state the cis−trans isomerization of *c*-APE in toluene involves efficient adiabatic one-way cis → trans torsional displacement over a 4.4 kcal/mol barrier in ^1c-APE$_B$* only. This conformer-specific reaction is a striking example of Havinga's nonequilibration of excited rotamers (NEER) principle.[29] It is remarkable in that it illustrates conformer-specific reactivity that arises not from structurally imposed proximity of the nuclei involved in bond-breaking or -making, as is the usual case, but from profound conformer-controlled differences in electronic distribution. It is these differences in electronic distribution that also account for the conformer-specific photocyclization of ^1c-APE$_A$*.[25] Structural considerations alone do not explain the different propensities of ^1c-APE$_A$* and ^1c-APE$_B$* toward cis → trans photoisomerization. On the contrary, the steric interactions that militate against the planar geometry in *cis*-stilbenes and provide the driving force for torsional relaxation in S_1 of such molecules appear to be more severe in ^1c-APE$_A$* than in ^1c-APE$_B$*. In addition to the usual ortho hydrogen interaction, in ^1c-APE$_A$* we have the proximity of a meta hydrogen of the phenyl group to the peri hydrogen at the 9-position of the anthracene moiety. Whether conformer control of electronic distribution plays a role in the reactivity of photobiological systems remains to be established. It is intriguing that the double bond of the cyclohexene moiety of the retinyl chromophore is s-cis to the acyclic double bond in rhodopsin but s-trans in bacteriorhodopsin.[30] The efficient double bond photoisomerization that is triggered by light in these two systems is in different directions and exhibits different regiochemistry.

Acknowledgment. This research was supported by NSF, most recently, by Grant CHE-9612316.

JA972293A

(28) Saltiel, J.; Ganapathy, S.; Werking, C. *J. Phys. Chem.* **1987**, *91*, 2755−2758.

(29) For a review see: Jacobs, H. J.; Havinga, E. *Adv. Photochem.* **1979**, *11*, 305−373.

(30) For a review see: Birge, R. R. *Biochim. Biophys. Acta* **1990**, *1016*, 293−327.